PHYSICAL REVIEW C VOLUME 3, NUMBER 2 FEBRUARY 1971

Neutron Total Cross Sections, 2.5–15 MeV. II. Effects of Nuclear Deformation*

Dale W. Glasgow†
Pacific Northwest Laboratory, Battelle Memorial Institute, Richland, Washington 99352 and Aerospace Research Laboratories, Wright-Patterson Air Force Base, Ohio‡ 45433

and

D. Graham Foster, Jr.§
Pacific Northwest Laboratory, Battelle Memorial Institute, Richland, Washington 99352

(Received 2 January 1970)

A spherical nonlocal optical-model analysis was performed on a homogeneous set of moderate-precision neutron total cross sections for 78 elements and 14 separated isotopes. The presence of fluctuations in the cross sections prevents the effective application of the optical model for nuclei with $A < 45$ unless the data are averaged over many experimental resolution widths. The dependence of the magnitude of the fluctuations on the ground-state spin of the target nucleus was observed. The analysis of the data for 46 spherical or soft nuclei within the regions $46 \leq A \leq 150$ and $188 \leq A \leq 206$, 2 transitional nuclei within the region $185 \leq A \leq 187$, and 19 hard-deformed nuclei within the regions $152 \leq A \leq 184$ and $228 \leq A \leq 239$ clearly indicates the effects of nuclear deformation. The spherical nonlocal optical potential of Perey and Buck describes (within 3%) the interaction of fast neutrons ($3.0 \leq E_n \leq 15.0$ MeV) with 46 spherical or soft nuclei. The analysis yields considerably less accurate (17%) results for the 19 hard-deformed nuclei. The surface thickness is approximately the same for all spherical nuclei (with the possible exception of light nuclei below $A = 46$), to the extent that the nonlocal optical potential has the same form as the nuclear-matter distribution. The systematic nature of the deviations of the data from the theoretical predictions leads to a conjecture which spans the mass range $45 \leq A \leq 239$.

I. INTRODUCTION

In a previous paper[1] (hereafter called I) we reported on a large-scale, homogeneous, moderate-precision measurement of neutron total cross sections for 78 naturally occurring elements and 14 separated isotopes spanning the energy range $2.25 \leq E_n \leq 15.0$ MeV. The measurements included all of the elements from hydrogen to plutonium, with the exception of the six inert gases and the highly radioactive elements in the vicinity of radium. In I we discussed the experimental method and technique, with emphasis on the precautions taken to minimize statistical and systematic errors. The large homogeneous set of data revealed a number of systematic phenomena resulting from the neutron-nucleus interaction taken over the above energy range and the mass-number range $1 \leq A \leq 239$. A three-dimensional Barschall plot of σ_T *versus* E_n *versus* $A^{1/3}$ exhibited continuous families of broad maxima and minima variously described as nonresonant Ramsauer structure or superpositions of scattering echoes. In addition to this broad structure, there was also a finer structure which was observable in the data for a number of the light nuclei. Interpretation of this structure will be reserved for future articles.

In previous papers[2,3] we addressed ourselves to the problem of probing the nuclear shape by means of a spherical nonlocal optical-model analysis of our neutron total cross-section data. This paper represents the logical continuation of that analysis. We emphasize the point that the large range in energy and mass number of the data imposes severe constraints upon any theoretical analysis. Furthermore, the existence of any deviations and systematic trends should be revealed, since this large block of homogeneous data has been subjected uniformly to any unknown systematic errors.

In this paper the phenomenological spherical nonlocal optical potential of Perey and Buck[4] is utilized to analyze the interaction of 3–15-MeV neutrons with virtually all of the stable elements. It is observed that the analysis adequately describes the behavior of the total cross section for neutrons of energy 3.0–15 MeV incident upon spherical or soft nuclei with $A > 45$. However, it is equally clear that such an analysis yields considerably less accurate results for all permanently deformed nuclei.

II. THEORY

As is well known, a detailed description[5] of the interaction of a neutron with a target nucleus may be described by a formal $(A+1)$-particle Schrödinger equation. The result of expanding the $(A+1)$-particle wave function over both open and

closed channels is an infinite set of coupled-channel integrodifferential equations. The generalized optical potential which appears in these equations is intrinsically energy dependent, nonlocal, spherical or spheroidal, and complex valued. Since it is impossible to solve the infinite set of coupled-channel equations, approximations are in order. The simplest approximation considers only the wave function in the shape elastic channel, while the effects of all of the ignored channels are described by an effective neutron-nucleus interaction potential. In this paper we have used this simple approximation in order to investigate further the range of validity of the Perey-Buck phenomenological spherical nonlocal optical potential, preparatory to a more detailed coupled-channel analysis.

The integrodifferential Schrödinger equation for the relative motion of a neutron in the field of the nucleus may be written

$$\frac{-\hbar^2}{2M}\nabla^2\psi(\vec{r}) + \int V(\vec{r},\vec{r}')\psi(\vec{r}')d\vec{r}' = E\psi(\vec{r}) \ , \qquad (1)$$

where, in general, the kernel contains elements that are *spherical* or *spheroidal* as well as nonlocal. A nonlocal potential may be visualized as reflecting the correlations which exist in nuclear matter, wherein the presence of a nucleon at $\vec{r}$ influences the probability of finding another nucleon at $\vec{r}'$ in the vicinity of $\vec{r}$. This in turn modifies the energy of the nucleon at $\vec{r}$ and leads to a nonlocal potential energy function. The nonlocal potential acting on an incident neutron situated at $\vec{r}$ not only depends on $\vec{r}$ and $\vec{r}'$ but also on the wave function evaluated at other points $\vec{r}'$ near $\vec{r}$.

Perey and Buck[4] utilized a *spherical* separable form as an approximation to the nonlocal kernel and rewrote Eq. (1) as

$$\frac{-\hbar^2}{2M}\nabla^2\psi(\vec{r}) + V_{so}S(r)\vec{l}\cdot\vec{\sigma}\psi(\vec{r}) + \int V_N(\vec{r},\vec{r}')\psi(\vec{r}')d\vec{r}' = E\psi(\vec{r}) \ , \qquad (2)$$

where the second term is a spherical local real spin-orbit potential of the Thomas form, and $V_N(\vec{r},\vec{r}')$ is a spherical nonlocal complex potential of the form $V(\frac{1}{2}|\vec{r}+\vec{r}'|)\delta(|\vec{r}-\vec{r}'|)$. The nonlocal function $\delta(|\vec{r}-\vec{r}'|)$ was described by a normalized Gaussian of the form

$$\delta(|\vec{r}-\vec{r}'|) = \pi^{-3/2}\beta^{-3}e^{-(|\vec{r}-\vec{r}'|/\beta)^2} \ , \qquad (3)$$

where β is the range of the nonlocality. They also set

$$-V(\tfrac{1}{2}|\vec{r}+\vec{r}'|) = Vf(p) + iW_d f_d(p) \ , \qquad (4)$$

where $p = \frac{1}{2}|\vec{r}+\vec{r}'|$.

In Eq. (4), the first term is a real potential and the second is an imaginary surface-interaction potential. The real spin-independent potential has a Woods-Saxon form

$$f(p) = [1 + e^{(p-R)/a_s}]^{-1} \ , \qquad (5)$$

and the imaginary potential has a derivative Woods-Saxon form

$$f_d(p) = 4e^{(p-R)/a_d}[1 + e^{(p-R)/a_d}]^{-2} \ . \qquad (6)$$

In Eqs. (5)–(7), $R = r_0 A^{1/3}$, where r_0 is the radius parameter; and a_s and a_d are the diffuseness parameters of the real and imaginary potentials.

The imaginary surface-interaction potential describes in a phenomenological sense the interaction of the incident neutron with the strongly interacting nuclear surface. This interpretation is approximately correct, since deep inside the nucleus nucleon collisions are inhibited by the Pauli exclusion principle, but this inhibition is relaxed near the surface due to the reduction of the Fermi momentum.[6]

Certain nuclei exhibit collective degrees of freedom. Those degrees of freedom corresponding to rotation and/or vibration of the nuclear surface may be predominantly excited by the incident neutron when it is near the nuclear surface. The relevance of this interpretation will become clear when we discuss the highly deformed rare-earth and actinide nuclei.

We have not used an imaginary volume absorption term in Eq. (4), since the Pauli principle will tend to preclude interaction of the incident neutron with the nucleons of the core for the energies under consideration in this study.

We have retained the real spin-orbit potential in the calculation of the total cross section, since the spin-orbit potential is also produced by a surface interaction.[6] In the interior of the nucleus, where the nucleon density is constant, the only direction having local significance is that associated with the momentum of a particle; hence, it is quite difficult to define a physically meaningful pseudovector that can be coupled to the nuclear spin. However, in the region of the nuclear surface the nucleon density gradient may be used to define uniquely the radial direction. A local spin-dependent potential may be formed from the density gradient, particle momentum, and the spin. If the range of the nuclear force is greater than the distance over which the nuclear density changes appreciably, the density variation in the nuclear surface suggests that the spin-orbit potential may have a slightly different radial variation. Nevertheless, most of the interaction will still be concentrated at or near the nuclear surface.

The Thomas form of the spin-orbit potential, which emphasizes the surface nature, is given by

$$S(r) = \left(\frac{\hbar}{2m_\pi c}\right)^2 \frac{1}{a_s r} e^{(r-R)/a_s} [1 + e^{(r-R)/a_s}]^{-2} . \quad (7)$$

An imaginary spin-orbit potential is not necessary for $E_n < 50$ MeV. The results of calculations of $\sigma_T(E, A)$ made with and without the spin-orbit interaction indicate a difference of about 0.5%. However, since portions of the experimental data were taken to a precision of 0.5%, the spin-orbit interaction cannot be neglected in this calculation.

With the energy dependence of the neutron total cross section approximately accounted for by the nonlocal potential and the surface properties by the surface imaginary and spin-orbit potentials, we can apply the model to the data and search for any deviations of the nuclear surface from a spherical shape.

Spherical and hard-deformed nuclei retain their shapes for long periods of time; only their orientations change, with all orientations equally probable. The nuclear-matter distribution corresponding to a randomly oriented, hard-deformed nucleus will exhibit a nonabrupt falloff to zero, even if the matter distribution has an abrupt edge. Since the matter distribution probably has a diffuse edge, the associated spherical distribution, after random averaging of the orientation, will exhibit a more diffuse edge. In contrast, the nuclear-matter distribution corresponding to a randomly oriented spherical nucleus will exhibit a less diffuse edge. Consequently, the nonlocal optical potential associated with the matter distribution of a hard-deformed nucleus will exhibit a more diffuse surface dependence, with a radius and surface thickness greater than that for neighboring spherical nuclei.

A large amount of experimental evidence indicates that permanently or hard-deformed nuclei (as discussed in Sec. III) exist quite generally throughout the nuclear periodic table, especially in those regions remote from closed neutron or proton shells. The regions D of Fig. 1, in which permanently deformed nuclei are most clearly recognized, are in the vicinity of $A = 8$, $18 \leq A \leq 28$, $50 < (Z \text{ or } N) < 82$, $152 \leq A \leq 186$ (rare earths), and $222 \leq A$ (actinides). The remaining regions are the domains of the spherical and vibrational or soft nuclei. However, even here the excited states of a number of nuclei have been interpreted in terms of a combination of spherical shapes, statically deformed shapes, and a dynamical deformation of the nuclear surface around the spherical equilibrium shape (soft nuclei).

For the case of *spherical nuclei*, Perey and Buck[4] observed fairly good agreement between their theoretical predictions and the existing neutron total cross-section data at 4.1, 7.0, 14.5, and 24.0 MeV. However, at the time of their analysis data were essentially nonexistent for nuclei in the deformed rare-earth region and for various members of the deformed actinide region. Consequently, the detailed behavior of the cross sections was not known for *hard-deformed* nuclei.

In the vicinity of 1–3 MeV, the total cross section for the interaction of a neutron with a hard-deformed nucleus will consist mainly of contributions due to direct elastic scattering from the deformed ground state, direct inelastic excitation of the rotational and vibrational states, compound-nuclear elastic scattering, and compound-nuclear inelastic scattering. As the neutron energy is increased above 4 MeV, the elastic and inelastic cross sections will be dominated by the direct interactions, while the compound-nuclear contributions will be diminished. This state of affairs will continue up to the $(n, 2n)$ threshold, which is in the vicinity of 7–8 MeV for the hard-deformed rare-earth nuclei. The $(n, 2n)$ cross section for typical rare-earth nuclei will be of the order of 20% of σ_T at 10 MeV and 30% at 14 MeV. Consequently, the total cross section spanning the energy range 4–14 MeV will consist mainly of direct elastic scattering from the deformed ground state and direct inelastic excitation of the rotational and vibrational states. The effects of the $(n, 3n)$ reaction will be negligible below 15 MeV. The situation for the highly deformed actinide nuclei is somewhat more complicated due to the fission process; however, the neutron scattering will still indicate whether the neutron is moving in a deformed or

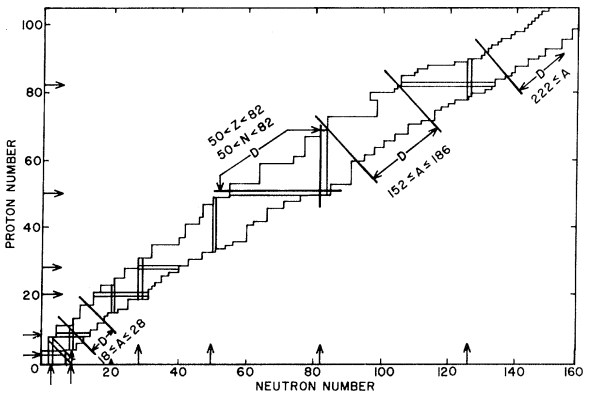

FIG. 1. A schematic representation of the nuclear Periodic Table. The arrows designate the closed neutron and proton shells at 2, 8, 20, 28, 50, 82, and 126. The regions marked D contain nuclei that exhibit permanently deformed shapes in the ground state.

spherical potential. Since the scattering processes typically provide the major contributions to the neutron total cross section, quantitative effects of nuclear deformation should be easily observed in moderate-precision (0.5–2.0%) total cross-section data.

III. ANALYSIS OF DATA

We have assumed in this article that the phenomenological spherical nonlocal optical potential of Perey and Buck provides approximately the correct energy variation of the neutron total cross sections for all spherical nuclei over the energy range of this experiment, and any gross deviations of the theory from the data may be correlated with the nuclear shape. Specifically, we searched for deviations in the regions $50 < (Z \text{ or } N) < 82$, $152 \leq A \leq 186$, and $222 \leq A \leq 240$. As we mentioned before, the spectra of nuclei in these regions correspond to states formed by collective vibrations and rotations of the nucleus. Since these states may be considered to arise from deformed nuclei, the associated optical potential will also exhibit a deformed nature.

Due to the magnitude of our data set, and the fact

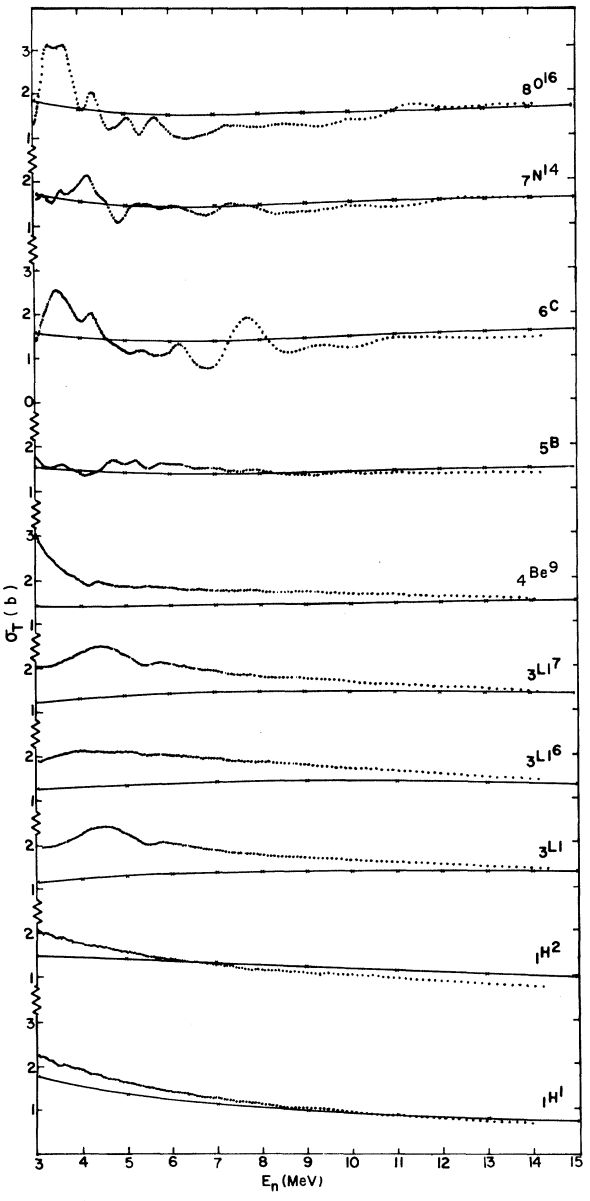

FIG. 2. Experimental and theoretical neutron total cross sections versus neutron energy for various 1s and 1p shell nuclei. The dots are seven-channel averages of the experimental data. The magnitude of the standard deviations associated with the data are ≤ the size of the dots.

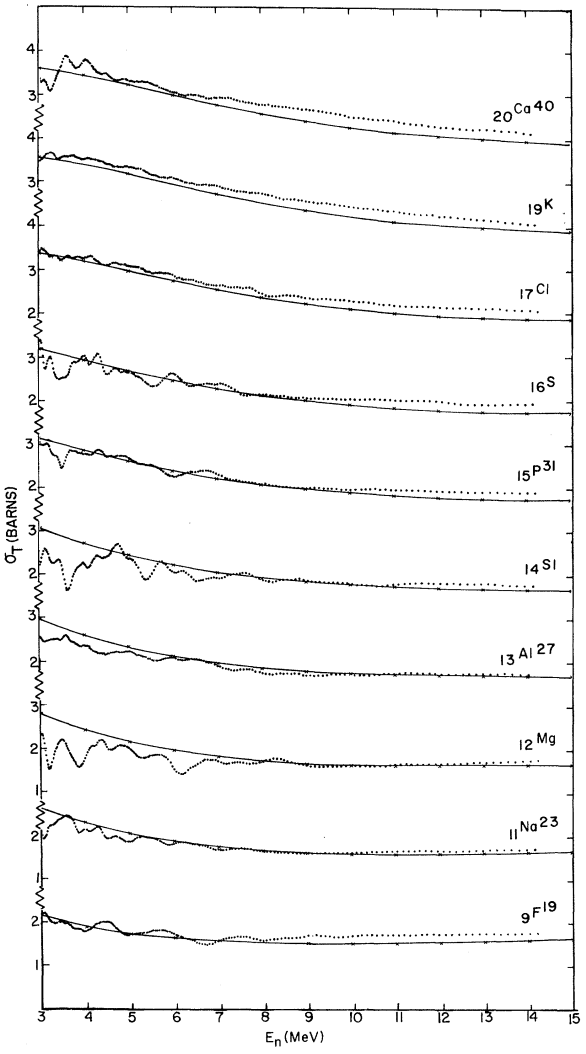

FIG. 3. Experimental and theoretical neutron total cross sections versus neutron energy for various 2s–1d shell nuclei. See caption for Fig. 2.

that Perey and Buck observed good agreement between their theoretical predictions and the existing data, and the fact that a limited parameter search gave values nearly equal to those of Perey and Buck, we did not perform a major parameter search but used the *single set of parameters* of Perey and Buck.[4]

The neutron total cross sections were calculated, using an IBM-7090 digital computer, at 14 energies spanning the energy range 3.0 to 15.0 MeV for all of the measured 78 elements and 14 separated isotopes using only this *one set of parameters*. The optical parameters were $V = 71$ MeV, $W_d = 15$ MeV, $V_{so} = 7.2$ MeV, $r_0 = 1.22$ fm, $a_s = 0.65$ fm, $a_d = 0.47$ fm, and $\beta = 0.85$ fm.

The comparisons of the data with the theoretical predictions are shown in Figs. 2–11. The solid curves are the theoretical results, while the points are sliding seven-channel averages (two resolution widths) of the experimental cross sections; i.e.,

$$\bar{\sigma} = \sum_{i=1}^{7} \frac{\sigma_i(E_i)\Delta E_i}{E_7 - E_1} \,. \tag{8}$$

The standard deviations are given by

$$(\mathrm{var}\bar{\sigma})^{1/2} = [(\underline{\Delta E})\underline{V}(\underline{\Delta E'})/(E_7 - E_1)^2]^{1/2} \,, \tag{9}$$

where $\underline{V}$ is the covariance matrix of the data, $\underline{\Delta E}$ is an energy row vector, and $\underline{\Delta E'}$ is its transpose. The covariance matrix of the data was discussed in I. The spatial extent of the standard deviations of the averaged total cross sections is less than the size of the points for practically all of the data below Rb.

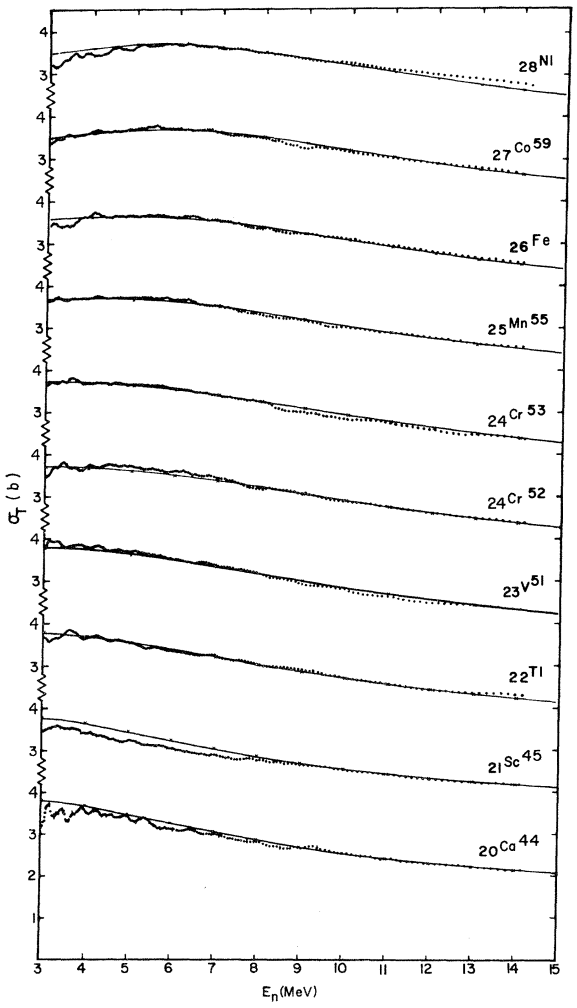

FIG. 4. Experimental and theoretical neutron total cross sections versus neutron energy for various $1f_{7/2}$ nuclei, with the exception of $_{20}Ca^{44}$. See caption for Fig. 2.

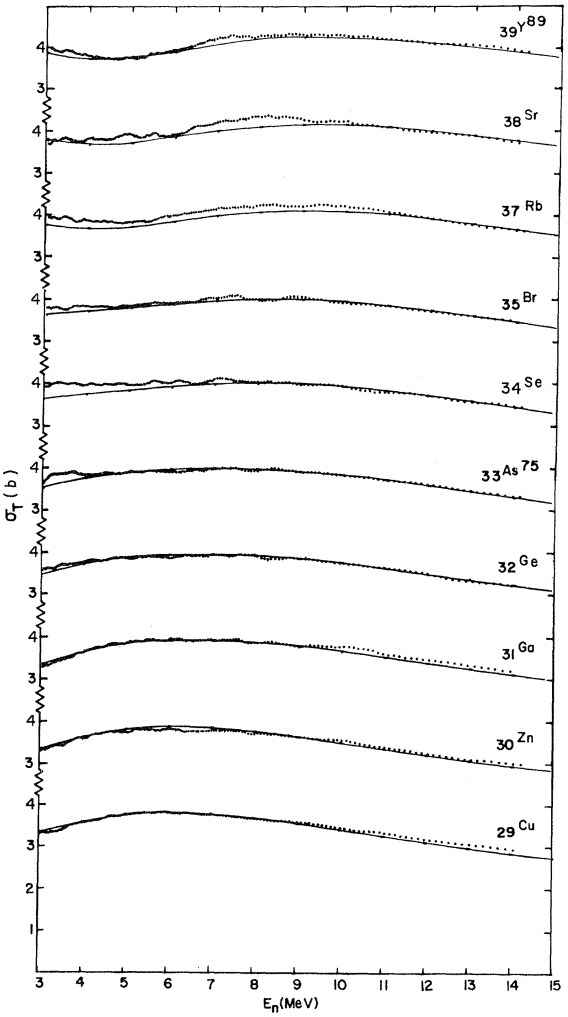

FIG. 5. Experimental and theoretical neutron total cross sections versus neutron energy for various $2p_{3/2}$, $1f_{5/2}$, and $2p_{1/2}$ nuclei. See caption for Fig. 2.

In Sec. III A–K we have tentatively listed the elements and separated isotopes for which we made measurements, according to where the ground states of their nuclei appear in the spherical shell-model sequence for protons. For deformed nuclei, the listing indicates the spherical states from which the deformed levels evolved. The exact filling order of the proton orbitals may ultimately be different from that listed.

A. $1s_{1/2}$, $1p_{3/2}$, $1p_{1/2}$ Nuclei;
$Z = 1$–8 ($_1H^1$, $_1H^2$, $_3Li$, $_3Li^6$, $_3Li^7$, $_4Be^9$, $_5B$, $_6C$, $_7N^{14}$, $_8O^{16}$)

In Fig. 2 we show the comparisons of the data for various light nuclei with the predictions of the spherical nonlocal optical model. Since this model has very limited, if any, validity in this mass region, we have used it here only to generate an average curve against which one may view the extreme structure in the neutron total cross sections. As an example, the plots indicate in a striking manner that the structure in the total cross section of natural $_3$Li is due to the interaction of the neutron with $_3Li^7$.

In order to describe the interaction of neutrons of these energies with such light nuclei as $_6C^{12}$, $_7N^{14}$, and $_8O^{16}$, one must perform a coupled-channel analysis similar to that reported by Tamura[7] and Reynolds *et al.*[8] The latter authors were able to calculate total cross sections for $_6C^{12}$ which agreed well with the available data over the energy range 0–5 MeV. The method used a real nonspherical local Woods-Saxon potential and allowed coupling between the ground and excited states of $_6C^{12}$. However, in order to fit the experimental data, the authors were compelled to use a coupling parameter β of the order of -0.04 to -0.08, as compared with a value of -0.6 obtained by Coulomb excitation. The implication was that the neutron does not fully sense the deformed ground-state equilibrium shape of $_6C^{12}$, but appears to be interacting primarily with a spherical nuclear field. In view of this rather surprising result, it would be enlightening to perform a similar calculation for $_8O^{16}$, taking into account the coexistence of the spherical ground state (0^+) and those deformed excited states which are built on the (0^+) state at 6.05 MeV.[9]

B. $1d_{5/2}$, $2s_{1/2}$, $1d_{3/2}$ Nuclei;
$Z = 9$–20 ($_9F^{19}$, $_{11}Na^{23}$, $_{12}Mg$, $_{13}Al^{27}$, $_{14}Si$, $_{15}P^{31}$ $_{16}S$, $_{17}Cl$, $_{19}K$, $_{20}Ca^{40}$, $_{20}Ca^{44}$)

Figure 3 shows the comparison of the σ_T data, with the theoretical predictions for various nuclei in the $2s$-$1d$ shell. It is apparent that the structure in the total cross sections produces extreme deviations from the simple optical model. The main difficulty in the analysis of the data lies in relating the effects of nuclear deformation or collective nuclear motion to the formation of states of the particle-hole type,[10] or the other possibility, unraveling the effects of nuclear deformation or collective nuclear motion from statistical fluctuations of the Ericson type.[11]

A number of examples illustrate the general nature of the deformed nuclei in this region. The low-lying $\frac{3}{2}^+$ and $\frac{5}{2}^+$ states of $_9F^{19}$ may be visualized, in the Nilsson scheme, as part of the rotational band built on the deformed ground state.[12] The spectra of two of the stable isotopes of magnesium, $_{12}Mg^{24}$ (79%) and $_{12}Mg^{25}$ (10%), display rotational band structure indicative of permanently deformed ground-state equilibrium shapes. The spectrum of the principal isotope of silicon, $_{14}Si^{28}$ (92%), appears to have an "inverted coexistence"[13] of the ground-state rotational band and the first excited (0^+) state (i.e., the *latter* may possess a spherical shape).

For the case of $_{16}S^{32}$ (95% of $_{16}S$), there exists the possibility of an inverted coexistence of the ground-state rotational band and the first excited (0^+) state; again the latter may possess a spherical equilibrium shape.[13] In addition,[9] coexistence of the spherical (0^+) ground state and deformed excited states built on the 3.348-MeV (0^+) level has been proposed to explain the 3.348- (0^+), 3.90- (2^+), and 5.62-MeV (4^+) levels in $_{20}Ca^{40}$.

If one takes the point of view that the fluctuations in the cross sections were the result of nuclear dynamics and were not statistical in origin, then the unified dynamical theory of nuclear reactions[5,14] may be used for the cross-section analysis. This is the optimistic approach, since it promises hope of predicting the amplitude, width, and energy position of the various structures in the cross sections. The data of experimental nuclear spectroscopy and the concepts of the nuclear collective model were extended to provide a description of nuclear reactions. Briefly, the technique was as follows: The transition matrix "T" was evaluated in terms of energy operators for, and connecting, the open and closed channels, and in terms of the scattering states associated with the average field encountered by the incident neutron in the open and closed channels. The scattering states were given in terms of particle-hole states in a collective-level scheme, and included the excitation of rotational or vibrational bands, where appropriate. Various authors have used this approach, with some success.[10,12]

If one takes the point of view that the fluctuations are statistical in origin, then a measure of the fluctuations is given by the variation of the σ_T around their average value. The variance may be

written[11]

$$\mathrm{var}[\langle\sigma_T(\epsilon,\Delta)\rangle] = \left[\frac{\pi\lambda^2}{2(2I+1)}\right]^2 \frac{2\Gamma^2}{\Gamma^2+\epsilon^2} \times \frac{1}{\pi\Gamma}\sum_J (2J+1)^2\rho^{-1}(E,J)\sum_l (T_{ls}^J)^2 , \quad (10)$$

where ϵ is an energy increment; Δ, the averaging energy interval for $\langle\sigma_T\rangle$; λ, the reduced wavelength of the incident neutron in the c.m. system; I, the ground-state spin of the target nucleus; Γ, the average level width; J, the spin of the compound-nuclear level; ρ, the density of nuclear levels of angular momentum J at an energy E above the completely degenerate state E_0; l and s, the orbital angular momentum and spin in the entrance channel; and T_{ls}^J is the transmission coefficient.

We pointed out in I that the greater the ground-state spin of the target nucleus, the smaller is the amplitude of the cross-section fluctuations and the lower the neutron energy at which they were no longer resolved in the experiment. An inspection of Eq. (10) indicates that the variance of σ_T is strongly influenced by the ground-state spin through the statistical weighting factor. The behavior of the weighting factor for the various experimental nuclei lying below, in, and just above the $2s$-$1d$ shell is illustrated in Table I. The fluctuations in the σ_T of ${}_6C^{12}(I=0)$ and ${}_8O^{16}(I=0)$ are greatly enhanced as compared with their neighbors ${}_5B(I=\frac{3}{2}, 3)$ and ${}_9F^{19}(I=\frac{1}{2})$. It is interesting to observe how similar are the unstructured cross sections of ${}_{17}Cl$ and ${}_{19}K$. The nuclei of both of these elements have $I=\frac{3}{2}$. In this prevailing spirit we can predict with confidence that the σ_T of the noble gases ${}_{10}Ne(I=0)$ and ${}_{18}Ar(I=0)$ will be heavily structured like their neighbors ${}_8O^{16}$, ${}_{12}Mg$, ${}_{16}S$, and ${}_{20}Ca^{40}$. There appears to be a strong qualitative correlation between the behavior of the data in Figs. 2–4 and Eq. (10). Since it is not our purpose in this paper to perform any detailed calculations involving the unified dynamical theory or the statistical theory, we will say little more on this subject.

A detailed view of Figs. 2–4 indicates that the predictions of the phenomenological spherical nonlocal optical model tend to agree better with the data for those nuclei possessing nonzero ground-state spins, i.e., for those nuclei in which nature has smoothed out the fluctuations. The smoothing results if there is competition among a large number of open channels. The number of open channels will increase as I increases. Since the structure for different channels and angular momenta is weakly correlated, very little structure will appear in the total cross sections.

Various authors have remarked from time to

TABLE I. Behavior of the statistical weighting factor as a function of the ground-state spin of the target nucleus.

Target nucleus	Ground-state spin (I)	Statistical weighting factor $1/[2(2I+1)]^2$
${}_5B$ (80% of nuclei have $I=\frac{3}{2}$)	$\frac{3}{2}$	$\frac{1}{64}$
${}_6C$ (99% of nuclei have $I=0$)	0	$\frac{1}{4}$
${}_7N^{14}$	1	$\frac{1}{36}$
${}_8O^{16}$	0	$\frac{1}{4}$
${}_9F^{19}$	$\frac{1}{2}$	$\frac{1}{16}$
${}_{11}Na^{23}$	$\frac{3}{2}$	$\frac{1}{64}$
${}_{12}Mg$ (90% of nuclei have $I=0$)	0	$\frac{1}{4}$
${}_{13}Al^{27}$	$\frac{5}{2}$	$\frac{1}{144}$
${}_{14}Si$ (95% of nuclei have $I=0$)	0	$\frac{1}{4}$
${}_{15}P^{31}$	$\frac{1}{2}$	$\frac{1}{16}$
${}_{16}S$ (99.2% of nuclei have $I=0$)	0	$\frac{1}{4}$
${}_{17}Cl$ (100% of nuclei have $I=\frac{3}{2}$)	$\frac{3}{2}$	$\frac{1}{64}$
${}_{19}K$ (99.1% of nuclei have $I=\frac{3}{2}$)	$\frac{3}{2}$	$\frac{1}{64}$
${}_{20}Ca^{40}$	0	$\frac{1}{4}$
${}_{20}Ca^{44}$	0	$\frac{1}{4}$
${}_{21}Sc^{45}$	$\frac{7}{2}$	$\frac{1}{256}$

time that one must be cautious in applying a single-channel optical-model analysis to nuclei with $A < 19$. In view of the abundant structure that still remains in the partially smoothed data of Fig. 3, we would add that this precaution should be extended up to $A \approx 45$, especially below an incident neutron energy varying from 7 or 8 MeV at $_9F^{19}$ to 5 MeV at $_{20}Ca^{44}$.

We will now progress on into regions of spherical and deformed nuclei, where nature has been kind and smoothed the cross sections. It is in such regions that the simple optical model may be used effectively in analyzing the data for effects of nuclear deformation.

C. Spherical or Vibrational $1f_{7/2}$ Nuclei; $Z = 21$–28 ($_{21}Sc^{45}$, $_{22}Ti$, $_{23}V^{51}$, $_{24}Cr^{52}$, $_{24}Cr^{53}$, $_{25}Mn^{55}$, $_{26}Fe$, $_{27}Co^{59}$, $_{28}Ni$)

Figure 4 shows the comparison of the σ_T data with the theoretical predictions for various nuclei in the $1f_{7/2}$ subshell, excluding $_{20}Ca^{44}$. A number of studies have been made in recent years in an attempt to understand the properties of nuclei in this shell in terms of the spherical shell model with a residual interaction between nucleons in a $1f_{7/2}$ configuration outside the closed shells. Specifically, the analysis of McCullen, Bayman, and Zamick[15] has explained a number of the properties of these nuclei, but has also given rise to questions regarding the behavior of odd-A nuclei in this region. However, it is sufficient to say that these nuclei can be considered to be approximately spherical or vibrational. This nomenclature includes oscillations of the nuclear surface about the spherical shape (soft nuclei).

A summary of the average fractional deviations of the data from the theoretical results is given in Table II. The average fractional deviation is defined as the arithmetic mean of $|\sigma_{ex} - \sigma_{theo}|/\sigma_{ex}$ taken at every 0.5-MeV interval spanning the energy region of interest. The variance of the average fractional deviation is 1 to 2 orders of magnitude smaller than the average fractional deviation. The nuclei are classified as spherical or soft, transitional, or hard deformed, according to the deviations of the experimental data from the theoretical predictions.

The grand-average deviation for $_{22}Ti$, $_{23}V^{51}$, $_{24}Cr^{52}$, $_{24}Cr^{53}$, $_{25}Mn^{55}$, $_{26}Fe$, $_{27}Co^{59}$, and $_{28}Ni$ is 1.1%. Furthermore, the disagreement is $\leq 1\%$ over 70% of the energy range, as expected. The major disagreement for $_{21}Sc^{45}$ may indicate dynamical deformation of the nucleus. It is known that ten energy levels are observed below 1.6 MeV for $_{21}Sc^{45}$, while the spherical shell-model calculations predict only one.[15] Most of the disagreement for $_{28}Ni$ (which should be spherical, since $Z = 28$) may be traced to the structure in the total cross section at lower energies. Since 98.9% of the nuclei of $_{28}Ni$ possess ground-state spins of $I = 0$, it is not surprising that the structure, and deviations from the spherical optical model, should result.

D. Spherical or Vibrational $2p_{3/2}$, $1f_{5/2}$, $2p_{1/2}$, $1g_{9/2}$ Nuclei; $Z = 29$–50 ($_{29}Cu$, $_{30}Zn$, $_{31}Ga$, $_{32}Ge$, $_{33}As^{75}$, $_{34}Se$, $_{35}Br$, $_{37}Rb$, $_{38}Sr$, $_{39}Y^{89}$, $_{40}Zr$, $_{41}Nb^{93}$, $_{42}Mo$, $_{43}Tc^{99}$, $_{44}Ru$, $_{45}Rh^{103}$, $_{46}Pd$, $_{47}Ag$, $_{48}Cd$, $_{49}In$, $_{50}Sn$)

Kisslinger and Sorenson[16] have studied many of the nuclei of these elements. They were able to give a consistent description of the nuclear properties by utilizing the pairing-plus-quadrupole model in which the sphericity-maintaining short-

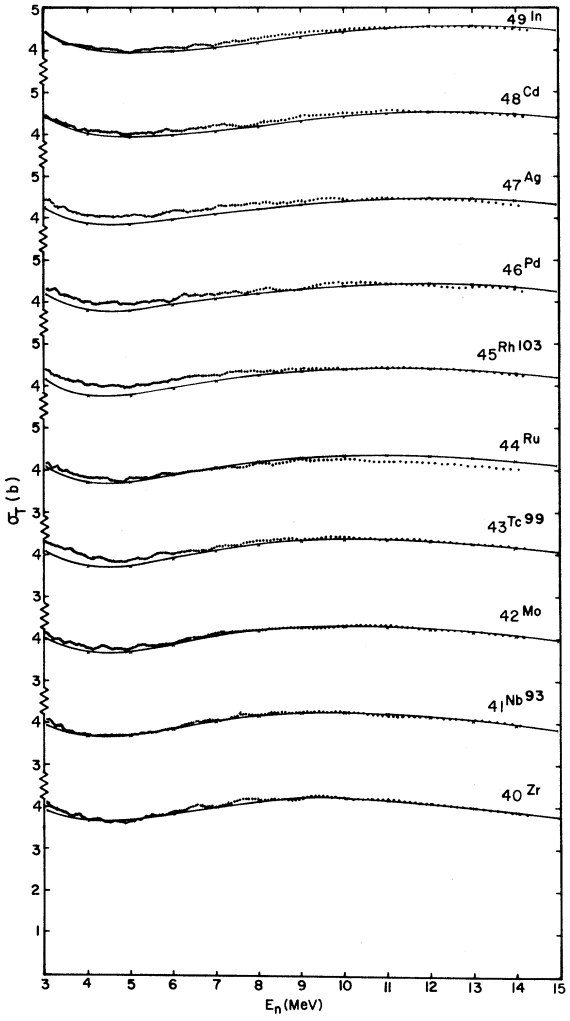

FIG. 6. Experimental and theoretical neutron total cross sections versus neutron energy for various $2p_{1/2}$ and $1g_{9/2}$ nuclei. See caption for Fig. 2.

TABLE II. Average fractional deviation of σ_T(experimental) from σ_T(theoretical). GA = grand average.

Element	Average fractional deviation (%) $3.0 \leq E_n \leq 15.0$ MeV	$3.0 \leq E_n \leq 6.0$ MeV	$6.0 \leq E_n \leq 15.0$ MeV
	Spherical or vibrational (soft) nuclei		
$_{21}Sc^{45}$	3.5		2.0
$_{22}Ti$	0.8		0.6
$_{23}V^{51}$	1.1		1.0
$_{24}Cr^{52}$	1.3		0.6
$_{24}Cr^{53}$	1.0		1.1
$_{25}Mn^{55}$	0.8		0.7
$_{26}Fe$	0.8		0.3
$_{27}Co^{59}$	0.9		0.6
$_{28}Ni$	2.0		1.9
$_{29}Cu$	1.1		1.4
$_{30}Zn$	1.4		1.3
$_{31}Ga$	1.5		1.7
$_{32}Ge$	0.9		0.5
$_{33}As^{75}$	0.7		0.2
$_{34}Se$	2.3		1.0
$_{35}Br$	1.2		0.5
$_{37}Rb$	2.8		2.3
$_{38}Sr$	2.7		2.5
$_{39}Y^{89}$	1.2		1.6
$_{40}Zr$	0.7		0.4
$_{41}Nb^{93}$	0.3		0.1
$_{42}Mo$	1.2		0.6
$_{43}Tc^{99}$	2.0		1.0
$_{44}Ru$	2.2		2.0
$_{45}Rh^{103}$	2.7		1.6
$_{46}Pd$	2.3		1.4
$_{47}Ag$	3.0		2.3
$_{48}Cd$	1.9		1.9
$_{49}In$	1.0		1.3
$_{50}Sn$	2.1		2.3
	GA 1.5		GA 1.2
	Soft nuclei		
$_{51}Sb$	2.7		3.2
$_{52}Te$	3.4		3.3
$_{53}I^{127}$	3.1		3.6
$_{55}Cs^{133}$	2.8		3.5
	GA 3.0		GA 3.4
$_{56}Ba$	4.8		5.6
	Spherical nuclei		
$_{57}La^{139}$	2.6		2.8
$_{58}Ce$	2.1		2.4
$_{59}Pr^{141}$	2.2		2.6
$_{60}Nd$	2.1		2.6
	GA 2.3		GA 2.6
	Hard-deformed nuclei		
$_{62}Sm$	6.0		7.5
$_{63}Eu$	7.2		8.4
$_{64}Gd$	6.3		7.6
$_{65}Tb^{159}$	5.8		7.0
$_{66}Dy$	7.1		9.3
$_{67}Ho^{165}$	6.0		8.0
$_{68}Er$	8.4		10.9
$_{69}Tm^{169}$	6.8		8.7
$_{70}Yb$	11.0		13.0

TABLE II *(Continued)*

Element	Average fractional deviation (%) $3.0 \leq E_n \leq 15.0$ MeV	$3.0 \leq E_n \leq 6.0$ MeV	$6.0 \leq E_n \leq 15.0$ MeV
$_{71}$Lu	6.1		7.5
	GA 6.6[a]		GA 8.3[a]
	Hard-deformed nuclei		
$_{72}$Hf	6.0		8.0
$_{73}$Ta^{181}	5.6		7.5
$_{74}$W^{182}	5.8		7.4
$_{74}$W	5.4		7.5
	GA 5.7		GA 7.6
	Transition nuclei		
$_{74}$W^{186}	4.2		5.4
$_{75}$Re	4.2		5.0
	GA 4.2		GA 5.2
	Spherical or vibrational (soft) nuclei		
$_{76}$Os	2.2		1.5
$_{77}$Ir	2.2		2.6
$_{78}$Pt	2.5		3.3
$_{79}$Au^{197}	2.4		2.5
$_{80}$Hg	3.1		4.0
$_{81}$Tl	3.1		2.6
$_{82}$Pb^{206}	3.0		2.5
	GA 2.6		GA 2.7
	Hard-deformed nuclei		
$_{90}$Th^{232}	5.8	7.5	6.4
$_{92}$U^{233}	6.6	8.1	7.7
$_{92}$U^{235}	6.8	8.3	7.9
$_{92}$U^{238}	7.2	8.5	7.8
$_{94}$Pu	7.8	9.6	8.7
	GA 6.8	GA 8.4	GA 7.7

[a]This grand average excludes $_{70}$Yb.

range pairing forces were stronger than the deforming long-range quadrupole forces. In view of their analysis, we have considered most of these nuclei to be approximately spherical or vibrational (soft).

The comparisons of the data and theoretical results are displayed in Figs. 5–7 and summarized in Table II. The grand-average deviation for these 21 elements and separated isotopes is 1.5%. Furthermore, the disagreement is <1.5% over 60% of the energy range for the nuclei of $_{29}$Cu, $_{30}$Zn, $_{31}$Ga, $_{32}$Ge, $_{33}$As^{75}, $_{35}$Br, $_{39}$Y^{89}, $_{40}$Zr, $_{41}$Nb^{93}, $_{42}$Mo, $_{48}$Cd, $_{49}$In, and $_{50}$Sn. However, we must comment on the anomalous behavior of $_{33}$As^{75}, $_{34}$Se, $_{37}$Rb, $_{38}$Sr, $_{43}$Tc^{99}, $_{44}$Ru, $_{45}$Rh^{103}, $_{46}$Pd, and $_{47}$Ag. It was pointed out in I that the data for $_{33}$As^{75} are probably correct over the energy region 4–15 MeV; however, the data may be incorrect over the energy range 3–4 MeV. Consequently, the deviations between 3 and 4 MeV should be viewed with some caution. Likewise, we suspect a possible error in the sample purity or thickness for $_{44}$Ru – hence the deviations over the entire energy range should also be considered with some caution. Nevertheless, we have retained the results, since they are qualitatively consistent and are within 3–4% of being quantitatively consistent. We have little reason to suspect any of the data for $_{34}$Se, $_{37}$Rb, $_{38}$Sr, $_{43}$Tc^{99}, $_{45}$Rh^{103}, $_{46}$Pd, and $_{47}$Ag (strontium required a correction for oxygen contamination, but the corrected data are consistent with the other six elements). The maximum deviations for these seven cases are of the order of 5% below 5–8 MeV. Such behavior may signal the presence of effects due to soft or vibrational nuclei. The Nilsson model predicts a closed shell with zero nuclear deformation at Z or $N = 40$. A close examination of Table II and Figs. 5–7 suggests that the minimum deviations occur near $_{40}$Zr, while the maximum deviations occur for the nuclei of $_{34}$Se, $_{37}$Rb, and $_{38}$Sr, which lie

between the $Z = 28$ and $Z = 40$ shells; and the nuclei of $_{43}Tc^{99}$, $_{44}Ru$, $_{45}Rh^{103}$, $_{46}Pd$, and $_{47}Ag$, which lie between the shells $Z = 40$ and $Z = 50$. It is reasonable to expect nonspherical nuclei away from closed shells.

The excellent agreement between the data and the theoretical results for the nuclei of $_{22}Ti$, $_{23}V^{51}$, $_{24}Cr^{52}$, $_{24}Cr^{53}$, $_{25}Mn^{55}$, $_{26}Fe$, $_{27}Co^{59}$, $_{28}Ni$, $_{29}Cu$, $_{30}Zn$, $_{31}Ga$, $_{32}Ge$, $_{33}As^{75}$, $_{35}Br$, $_{39}Y^{89}$, $_{40}Zr$, $_{41}Nb^{93}$, $_{42}Mo$, $_{48}Cd$, $_{49}In$, and $_{50}Sn$ supports the previous assumption that the spherical nonlocal optical potential of Perey and Buck[4] adequately describes the energy variation of nature-smoothed neutron total cross sections for spherical nuclei, as expected. In addition, the surface thickness is about the same for all of these nuclei, to the extent that the nonlocal optical potential has the same form as the nuclear-matter distribution.

E. $1g_{7/2}$ Nuclei; Deformed Region

$50 < (Z \text{ or } N) < 82$ ($_{51}Sb$, $_{52}Te$, $_{53}I^{127}$, $_{55}Cs^{133}$)

Sheline, Sikkeland, and Chanda[17] were the first to present experimental evidence for a region of nuclear deformation among the highly neutron-deficient nuclei in the region $50 < (Z \text{ or } N) < 82$ of Fig. 1. By observing the systematic lowering of the

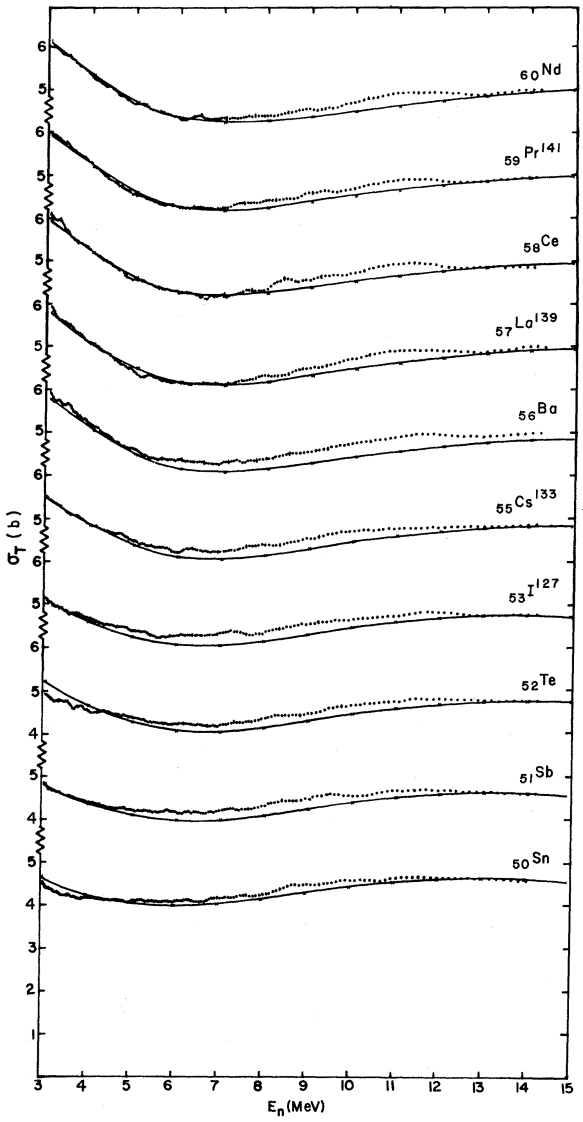

FIG. 7. Experimental and theoretical neutron total cross sections versus neutron energy for various $1g_{7/2}$ and $2d_{5/2}$ nuclei. See caption for Fig. 2.

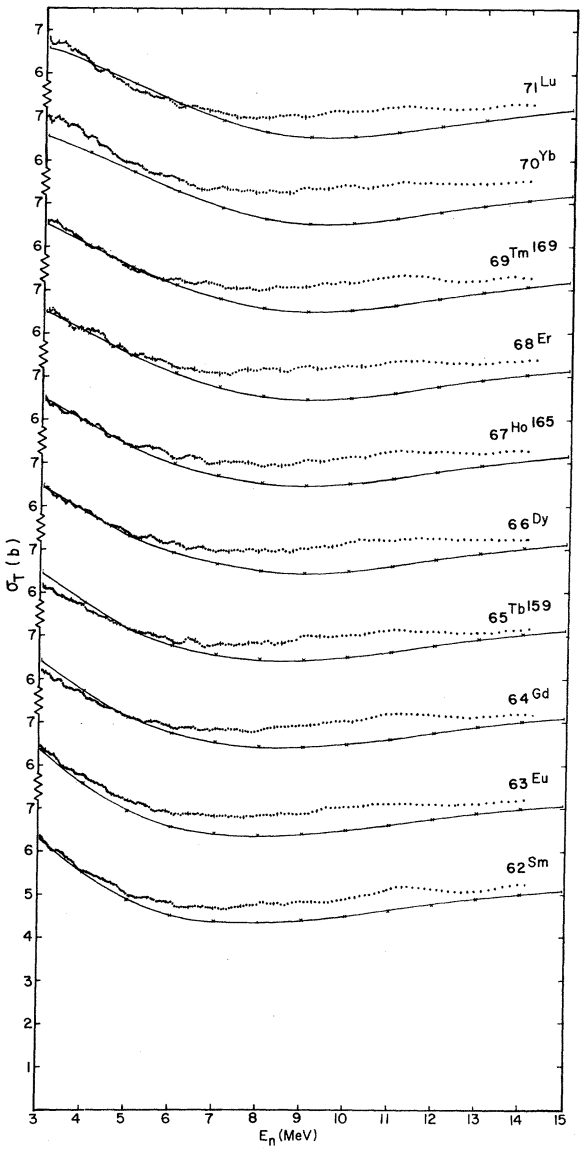

FIG. 8. Experimental and theoretical neutron total cross sections versus neutron energy for various $2d_{5/2}$ and $1h_{11/2}$ nuclei. See caption for Fig. 2.

first excited states in even-even $_{56}Ba^{126-130}$ nuclei they concluded that certain barium nuclei were deformed. Marshalek, Person, and Sheline[18] were among the first to predict that additional deformed nuclei should exist in this region of the nuclear periodic table. The nature of the equilibrium deformation was obtained by minimizing the sum of the eigenvalues of the Nilsson-model Hamiltonian for a particular configuration and deformation parameter.

Kumar and Baranger[19] performed an analysis, based on the pairing-plus-quadrupole model of nuclear forces, indicating that the equilibrium nuclear shapes were oblate for neutron-deficient nuclei in this region. A quadrupole deformation potential was added to the spherical-shell-model Hamiltonian to give a deformed Hamiltonian. The single-particle levels and wave functions were calculated for all possible values of the static and dynamic deformation parameters. For each choice of the deformation parameters, the pairing force was used to do a BCS calculation on the single-particle levels. The expectation value of the pairing-plus-quadrupole Hamiltonian was calculated using the BCS wave functions. The absolute minimum of the expectation value for a particular set of deformation parameters gave the equilibrium shape. If the expectation value had a sharp minimum, the nucleus was considered to be hard deformed. If the minimum was shallow, the nucleus possessed vibrational aspects, and was said to be soft. Ackermann *et al.*[20] have presented experimental evidence that indicated the neutron-deficient nuclei $_{55}Cs^{131,132}$ were indeed deformed in an oblate manner.

In Fig. 7 the nuclei of $_{51}Sb$, $_{52}Te$, $_{53}I^{127}$, and $_{55}Cs^{133}$ lie within the deformed region $50 < (Z \text{ or } N) < 82$. Neither $_{53}I^{127}$ nor $_{55}Cs^{133}$ possess rotational spectra, so we consider them to be spherical or soft. A similar statement applies to the nuclei of the major isotopes of $_{51}Sb$ and $_{52}Te$ (data possibly unreliable, see I). Consequently, we do not attribute the 5% maximum and 3.0% grand-average deviations to hard nuclear deformation. We contend that the nuclei of the major stable isotopes of these four elements are not sufficiently neutron deficient to be permanently deformed, at least to the extent required here for detection; however, they may be soft.

F. Spherical $1g_{7/2}$, $2d_{5/2}$ Nuclei; $N \geq 82$ ($_{56}Ba$), ($_{57}La^{139}$, $_{58}Ce$, $_{59}Pr^{141}$, $_{60}Nd$)

Since 50 and 82 are good magic numbers, it is reasonable to believe that the properties of nuclei with $N = 82$ and $Z \geq 50$ may be described by a spherical shell model. Consequently, we have assumed that these nuclei possess a spherical equilibrium shape. The nuclei of the major stable isotope of Ba (71.7% $_{56}Ba^{138}$), $_{57}La^{139}$, the major stable isotope of Ce (88.5% $_{58}Ce^{140}$), and $_{59}Pr^{141}$ fall within this spherical category with $N = 82$ and $Z > 50$. In addition, these nuclei do not show the rotational band structure which is the hallmark of deformed nuclei.

On the other hand, 73% of the nuclei of the stable isotopes of $_{60}Nd$ lie within the complicated transition region beyond the $N = 82$ magic neutron shell and before the highly deformed region $152 \leq A \leq 186$ of Fig. 1. The level structure of these nuclei is difficult to interpret solely from the standpoint of a spherical shell model due to the complexity of the shell-model states. A more successful interpretation involves a description which utilizes Nilsson-model configurations with a small amount of deformation. However, an observation of the average fractional deviations of Table II suggests that the nuclei of $_{60}Nd$ can be considered approximately spherical.

A study of Fig. 7 and Table II reveals that $_{56}Ba$ presents an anomaly. The data lie everywhere above the theoretical predictions with an average fractional deviation of 4.8%, as compared with 2.6% for its neighbor $_{57}La^{139}$. To our knowledge, there are no systematic errors in the data, so perhaps nature is trying to reveal itself. However, in view of this anomaly we have not placed $_{56}Ba$ into either of the categories of Secs. III E or F.

The experimental and theoretical predictions for the nuclei of the other four elements (see Fig. 7 and Table II) tend to agree to within 1–4%, with a grand-average deviation of 2.3%, which is consistent with their description as spherical nuclei. The surface thickness appears to be the same for these nuclei, within the approximation that the nonlocal optical potential has the same form as the nuclear-matter distribution.

G. $2d_{5/2}$, $1h_{11/2}$ Hard-Deformed Rare-Earth Nuclei; $152 \leq A \leq 186$ ($_{62}Sm$, $_{63}Eu$, $_{64}Gd$, $_{65}Tb^{159}$, $_{66}Dy$, $_{67}Ho^{165}$, $_{68}Er$, $_{69}Tm^{169}$, $_{70}Yb$, $_{71}Lu$)

One of the distinguishing characteristics of permanently or hard-deformed nuclei is the existence of rotational band structure in their energy-level diagrams. The energy spacing varies approximately as $I(I+1)$, where I is the total angular momentum of the rotor and its coupled particle. There are, however, deviations from this simple behavior when the projection K of the total angular momentum I on the symmetry axis is equal to $\frac{1}{2}$, 1, and $\frac{3}{2}$. The ground-state rotational bands of certain even-even nuclei, e.g., $_{4}Be^{8}$, $_{12}Mg^{24}$, $_{62}Sm^{154}$, $_{92}U^{238}$, provide us with some of the clear-

est examples of rotational structure. However, certain odd-A nuclei also exhibit rotational band structure, and with a higher density of levels. The rare-earth region $152 \leq A \leq 186$ of Fig. 1 provides us with many excellent examples. The comparisons of the data and theoretical results for the nuclei of $_{62}$Sm, $_{63}$Eu, $_{64}$Gd, $_{65}$Tb^{159}, $_{66}$Dy, $_{67}$Ho^{165}, $_{68}$Er, $_{69}$Tm^{169}, $_{70}$Yb, and $_{71}$Lu are displayed in Fig. 8 and summarized in Table II. The data for $_{62}$Sm deviate from the theoretical predictions by an overall average of 6% (which corresponds to six standard deviations of the experimental data) taken over the energy range 3–15 MeV. The difference reaches a maximum of 11% (nine standard deviations of the data). It is apparent from observation of the data for $_{60}$Nd and $_{62}$Sm that the gross deviations appear quite suddenly. This is consistent with the abrupt appearance of rotational band structure in the energy levels of $_{62}$Sm^{152} at $N = 90$. This isotope and $_{62}$Sm^{154} constitute 47% of natural $_{62}$Sm.

The deviations are also consistent with the predictions of Kumar and Baranger,[21] who have used the pairing-plus-quadrupole model to study the static nuclear shapes in the even-even samarium isotopes. They predicted an abrupt onset of deformation as the neutron number reaches 90; i.e., at $_{62}$Sm^{152}.

The deviations for $_{63}$Eu average 7.2%, taken over the energy range 3–15 MeV, with a maximum of 11.7%. Considering that natural $_{63}$Eu consists of a mixture of two isotopes, $_{63}$Eu^{153} ($N = 90$) and $_{63}$Eu^{151} ($N = 88$) with $_{63}$Eu^{153} comprising 52%, the deviations are again consistent with the results of nuclear spectroscopy and the predictions of Kumar and Baranger[21] for the sudden onset of deformation. Sakai[22] has performed an analysis of the energy-level structure of a number of the even-even $_{64}$Gd isotopes. It was observed that the excited 0^+, 2^+, 4^+, ... and 2^+, 3^+, 4^+, ... states may be considered to be quasi-β and quasi-γ bands. The relative location of the head states of the quasibands with respect to the first excited 2^+ state was found to be a much more sensitive measure of the onset of deformation than was the energy ratio of the second 4^+ state to the first 2^+ state. The onset of nuclear deformation was observed to occur between $_{64}$Gd^{152} ($N = 88$) and $_{64}$Gd^{154} ($N = 90$). In natural $_{64}$Gd, 99.8% of the nuclei have $N \geq 90$; consequently, the σ_T of $_{64}$Gd should also reflect the effects of nuclear deformation, as indeed we observe in Fig. 8 and Table II.

After the abrupt appearance of the effects of nuclear deformation, the deviations between the data and theoretical results level off. The average deviations taken over the energy range 3–15 MeV for the 10 elements, $_{62}$Sm–$_{71}$Lu, are 6.0, 7.2, 6.3, 5.8, 7.1, 6.0, 8.4, 6.8, 11.0, and 6.1%, respectively. These deviations are far beyond statistical fluctuations, since they correspond to 8–12 standard deviations of the data. The maximum deviations are 11.0, 11.7, 12.4, 12.4, 15.3, 14.1, 16.9, 14.5, 18.7, and 12.9%, respectively. These maximum deviations correspond to 8–17 standard deviations of the data. The 11.0 and 18.7% average and maximum deviations associated with $_{70}$Yb should be viewed with some caution, since we suspect a possible error in the sample purity or thickness. Nevertheless, we propose that the behavior of the deviations illustrates the qualitative behavior of the deformation for the nuclei of $_{70}$Yb and the quantitative behavior of the deformation for the nuclei of $_{62}$Sm, $_{63}$Eu, $_{64}$Gd, $_{65}$Tb^{159}, $_{66}$Dy, $_{67}$Ho^{165}, $_{68}$Er, $_{69}$Tm^{169}, and $_{71}$Lu.

Incidentally, our measurement of $\sigma_T(E)$ for $_{67}$Ho^{165} agrees to within 1% with the only known extensive measurement of $\sigma_T(E)$ for a hard-deformed rare-earth nucleus, namely, the measurements of Marshak *et al.*[23] These authors have applied a coupled-channel analysis to their data. The maximum deviation between their data and the theoretical results was 5% as compared with 14% for the present spherical nonlocal analysis.

H. $1h_{11/2}$ Deformed Nuclei; $Z = 72$–74 ($_{72}$Hf, $_{73}$Ta^{181}, $_{74}$W^{182}, $_{74}$W)

The nuclei of $_{72}$Hf, $_{73}$Ta^{181}, and $_{74}$W^{182} are located in the hard-deformed region, while the heavier nuclei of $_{74}$W are located near the beginning of the region over which nuclei change from a permanently deformed shape to a spherical shape. A view of Fig. 9 and Table II indicates that a gradual transition is taking place over this portion of the nuclear periodic table. The grand-average deviation between the data and the theoretical predictions taken over the energy range 3–15 MeV is 5.7%, as compared with 6.6% for the rare-earth group. The maximum deviations are of the order of 10%, as compared with 11–18% for the rare-earth nuclei. The preceding behavior is consistent with the slowly changing deformation.

I. $1h_{11/2}$ Transition Nuclei; $Z = 74$–75 ($_{74}$W^{186}, $_{75}$Re)

In this paper nuclei have been divided into spherical, soft, or deformed categories for the purposes of understanding and classification. However, this classification is not strictly applicable for transition nuclei, where deviations from a purely spherical, vibrational, or rotational description are significant. The stable nuclei of $_{74}$W^{186} and $_{75}$Re fall into the transition-nuclei category. A study of Table II and Fig. 9 indicates a

line of demarcation between the behavior of the nuclei of $_{74}W^{182}$ and $_{74}W^{186}$, with average and maximum deviations of 5.8 and 9.7% for $_{74}W^{182}$, and 4.2 and 6.8% for $_{74}W^{186}$, respectively. The addition of four neutrons to $_{74}W^{182}$ to form $_{74}W^{186}$ illustrates the behavior of the neutron pairing force, i.e., it favors spherical symmetry over axial symmetry. The behavior of $_{75}$Re, with average and maximum deviations of 4.2 and 7.0%, is also consistent with the changing deformation.

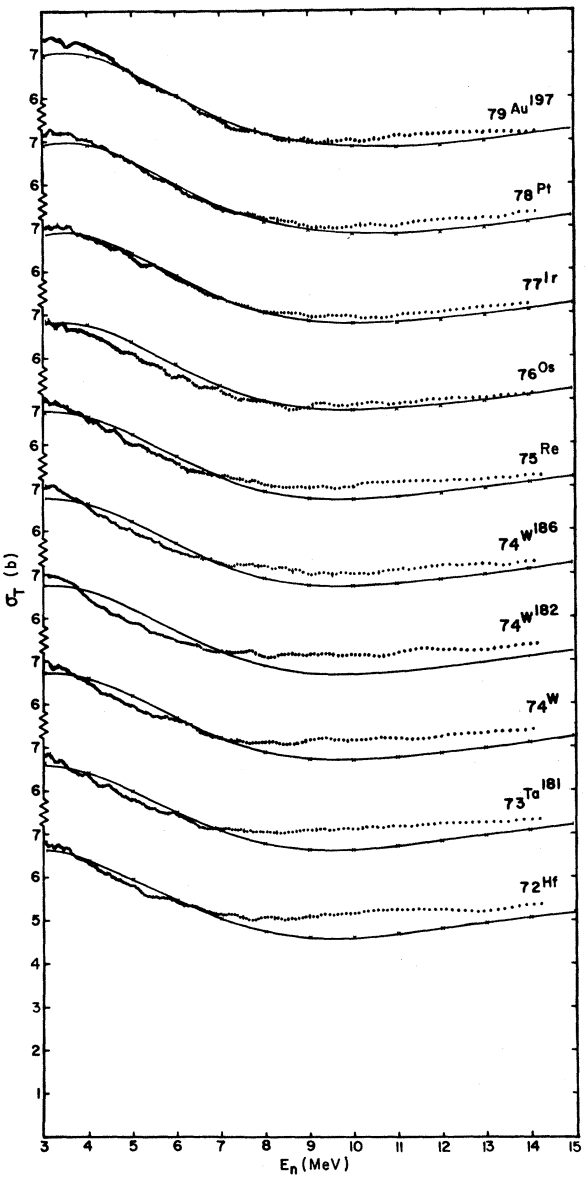

FIG. 9. Experimental and theoretical neutron total cross sections versus neutron energy for various $1h_{11/2}$ and $2d_{3/2}$ nuclei. See caption for Fig. 2.

J. $1h_{11/2}$, $2d_{3/2}$, $3s_{1/2}$ Spherical or Soft Nuclei; $Z = 76$–82 ($_{76}$Os, $_{77}$Ir, $_{78}$Pt, $_{79}$Au^{197}, $_{80}$Hg, $_{81}$Tl, $_{82}$Pb^{206})

The analysis of the even-even isotopes of $_{76}$Os by Sakai[22] revealed that the region of transition from deformed to spherical nuclei occurs less abruptly than the transition from spherical to deformed at $N = 90$. The transition occurs somewhere between $_{76}$Os^{186} and $_{76}$Os^{190}, i.e., $N = 110$–114, which is consistent with the analysis of Kumar and Baranger.[21] The latter analysis revealed the ascendancy of the sphericity-maintaining pairing force over the deforming quadrupole force, as pairs of neutrons were added to the nucleus. We propose that our σ_T measurements on natural $_{76}$Os were performed on essentially soft or spherical nuclei, since 97% of the stable nuclei of $_{76}$Os are included in the isotopic range $_{76}$Os^{188}–$_{76}$Os^{192}.

The analysis of Sakai[22] also revealed that the transition in $_{78}$Pt appears near $_{78}$Pt^{188}. In our total cross-section sample of $_{78}$Pt, the lightest stable isotope is $_{78}$Pt^{190}; consequently, our measurements were made on essentially soft or spherical nuclei of $_{78}$Pt.

Natural $_{77}$Ir consists of two stable isotopes, $_{77}$Ir^{191} (37%) and $_{77}$Ir^{193} (63%). In view of the fact that hard deformation has nearly vanished for $N = 116$ and that the vanishing occurs more rapidly as a function of Z, we view the nuclei of natural

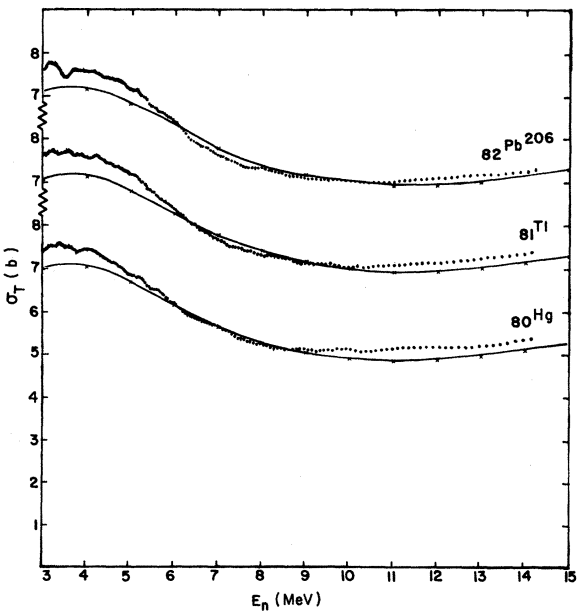

FIG. 10. Experimental and theoretical neutron total cross sections versus neutron energy for various $2d_{3/2}$ and $3s_{1/2}$ nuclei. See caption for Fig. 2.

$_{77}$Ir as soft or spherical. The same criterion applies, even more so, to the nuclei of $_{79}$Au^{197}, $_{80}$Hg, $_{81}$Tl, and $_{82}$Pb^{206}.

The average deviations between the data and the theoretical predictions are displayed in Figs. 9 and 10 and summarized in Table II. The maximum deviations between the data and the theoretical results for $_{80}$Hg, $_{81}$Tl, and $_{82}$Pb^{206} are of the order of 5%, while the average deviations are about 3%. These deviations may be compared with the maximum and average values of 4 and 2.3% for the spherical ($N=82$) nuclei of $_{57}$La^{139}, $_{58}$Ce, $_{59}$Pr^{141}, and $_{60}$Nd.

The grand-average deviation between the data and the theoretical results for the nuclei of $_{76}$Os, $_{77}$Ir, $_{78}$Pt, $_{79}$Au^{197}, $_{80}$Hg, $_{81}$Tl, and $_{82}$Pb^{206} is 2.6%, which is certainly consistent with their description as spherical or nearly spherical nuclei. In view of the fact that we have used the same surface-diffuseness parameters throughout the analysis, spanning the mass range $1 \leq A \leq 239$, it appears that the surface thickness is about the same for all spherical nuclei, with the possible exception of light nuclei. This conclusion is valid to the extent that the nonlocal optical potential has the same form as the nuclear-matter distribution.

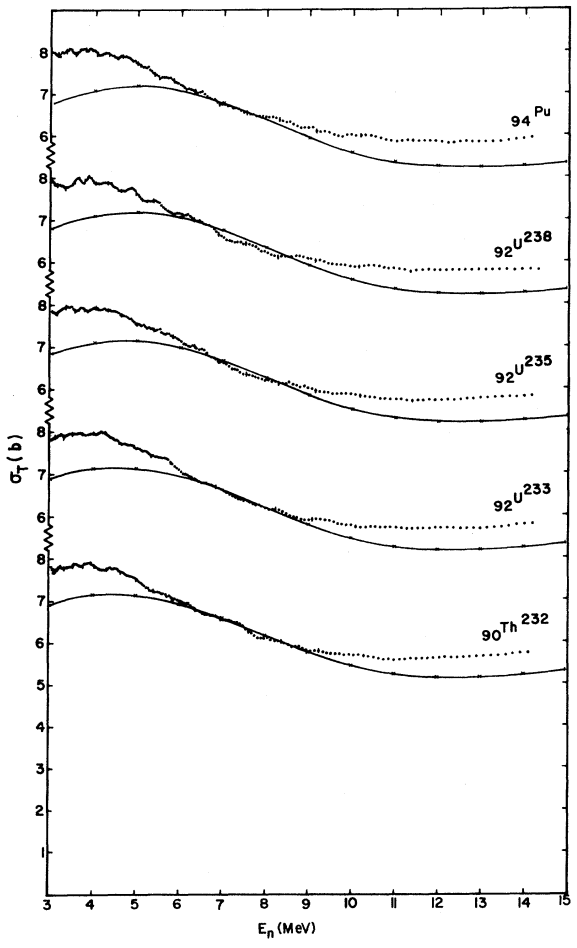

FIG. 11. Experimental and theoretical neutron total cross sections versus neutron energy for various $1h_{9/2}$ and $2f_{7/2}$ nuclei. See caption for Fig. 2.

K. $1h_{9/2}$, $2f_{7/2}$ Deformed Actinide Nuclei; $228 \leq A \leq 239$ ($_{90}$Th^{232}, $_{92}$U^{233}, $_{92}$U^{235}, $_{92}$U^{238}, $_{94}$Pu)

The well-developed rotational bands, and β and γ vibrational bands of $_{90}$Th^{232}, $_{92}$U^{233}, $_{92}$U^{235}, $_{92}$U^{238}, and $_{94}$Pu illustrate in a clear manner the collective structure of these nuclei. The deviations between the data and the predictions of the spherical nonlocal optical model are again dramatic and are shown in Fig. 11 and Table II. The grand-average deviation spanning the energy range 3–15 MeV is 6.8%, with maximum deviations of 17%. The behavior of the deviations is again consistent with the deformation in the region $228 \leq A \leq 239$.

IV. SUMMARY

The grand-average deviations between the experimental σ_T and the predictions of the spherical nonlocal optical model are:

(1) 1.5% for the spherical or soft nuclei of the stable isotopes of $_{22}$Ti, $_{23}$V^{51}, $_{24}$Cr^{52}, $_{24}$Cr^{53}, $_{25}$Mn^{55}, $_{26}$Fe, $_{27}$Co^{59}, $_{28}$Ni, $_{29}$Cu, $_{30}$Zn, $_{31}$Ga, $_{32}$Ge, $_{33}$As^{75}, $_{34}$Se, $_{35}$Br, $_{37}$Rb, $_{38}$Sr, $_{39}$Y^{89}, $_{40}$Zr, $_{41}$Nb^{93}, $_{42}$Mo, $_{43}$Tc^{99}, $_{44}$Ru, $_{45}$Rh^{103}, $_{46}$Pd, $_{47}$Ag, $_{48}$Cd, $_{49}$In, and $_{50}$Sn, which lie within the region $46 \leq A \leq 124$;

(2) 3.0% for the spherical or soft nuclei of the stable isotopes of $_{51}$Sb, $_{52}$Te, $_{53}$I^{127}, and $_{55}$Cs^{133}, which lie within the region $50 < (Z \text{ or } N) < 82$;

(3) 2.3% for the spherical nuclei of the stable isotopes of $_{57}$La^{139}, $_{58}$Ce, $_{59}$Pr^{141}, and $_{60}$Nd, which lie on or just beyond the $N=82$ neutron shell;

(4) 6.6% (excluding $_{70}$Yb) for the highly deformed nuclei of the stable isotopes of the rare earths $_{62}$Sm, $_{63}$Eu, $_{64}$Gd, $_{65}$Tb^{159}, $_{66}$Dy, $_{67}$Ho^{165}, $_{68}$Er, $_{69}$Tm^{169}, ($_{70}$Yb), and $_{71}$Lu, which lie within the region $152 \leq A \leq 184$;

(5) 5.7% for the highly deformed nuclei of the stable isotopes of $_{72}$Hf, $_{73}$Ta^{181}, $_{74}$W^{182}, and $_{74}$W, which lie within the region $152 \leq A \leq 184$;

(6) 4.2% for the transition nuclei of the stable isotopes of $_{74}$W^{186} and $_{75}$Re, which lie within the region $185 \leq A \leq 187$;

(7) 2.6% for the spherical or soft nuclei of the stable isotopes of $_{76}$Os, $_{77}$Ir, $_{78}$Pt, $_{79}$Au^{197}, $_{80}$Hg, $_{81}$Tl, and $_{82}$Pb^{206}, which lie within the region $188 \leq A \leq 206$;

(8) 6.8% for the highly deformed nuclei of the isotopes of the actinides $_{90}$Th^{232}, $_{92}$U^{233}, $_{92}$U^{235}, $_{92}$U^{238}, and $_{94}$Pu, which lie within the region $228 \leq A \leq 239$.

A briefer summary indicates that the deviations

are consistent with the:
(1) spherical or soft nature of the nuclei of 39 elements or separated isotopes within the region $46 \leq A \leq 150$;
(2) spherical or soft nature of the nuclei of seven elements or separated isotopes within the region $188 \leq A \leq 206$;
(3) transitional nature of the nuclei of two elements or separated isotopes within the region $185 \leq A \leq 187$;
(4) deformed nature of the nuclei of 14 elements or separated isotopes within the region $152 \leq A \leq 184$;
(5) deformed nature of the nuclei of five elements or separated isotopes within the region $228 \leq A \leq 239$.

V. CONCLUSIONS

A spherical nonlocal optical-model analysis of neutron total cross-section data for 46 spherical or vibrational, 2 transitional, and 19 highly deformed nuclei clearly indicates the presence or absence of the effects of nuclear deformation. The results of the analysis indicate that the surface thickness is about the same for all spherical nuclei with the possible exception of light nuclei. This conclusion is valid to the extent that the nonlocal optical potential has the same form as the nuclear-matter distribution.

It is clear that an analysis which uses the phenomenological spherical nonlocal optical potential of Perey and Buck adequately describes the behavior of the total cross section for fast neutrons ($3.0 \leq E_n \leq 15.0$ MeV) incident upon spherical nuclei heavier than $_{21}Sc^{45}$. This must be considered as an additional triumph for the Perey-Buck nonlocal potential model. However, it is equally clear that such an analysis yields considerably less accurate results for highly deformed nuclei. Presumably, if one could eliminate the effects of deformation upon the optical potential, the analysis would also be adequate for these nuclei. It is known that the effects of nuclear deformation upon the phenomenological optical potential can be eliminated artificially by explicitly treating the strong coupling between the ground and excited states in a coupled-channel analysis.[7,23-27]

We conjecture that when this contribution has been removed, the remaining effective nonlocal potential should adequately describe the total probability for the interaction of neutrons ($3.0 \leq E_n \leq 15.0$ MeV) with any of the nuclei within $45 \leq A \leq 239$ regardless of whether they are spherical or highly deformed. With the effective nonlocal potential determined by the behavior of the spherical nuclei in the regions $46 \leq A \leq 150$ and $188 \leq A \leq 206$, the nuclear-shape parameters β_i may be determined by a fit to the homogeneous high-precision neutron total cross-section data. Since there is no *a priori* reason for neutrons to sense the same component of the nuclear field as, say, α particles, it is conceivable that the deformation parameters determined by neutron and α-particle scattering may be different. This will be especially true if the matter and charge distributions of the nucleons are different, and also if the shape of the optical potential is not identical to the shape of nuclear matter.

We hope to investigate these questions by way of a coupled-channel analysis of the rare-earth σ_T data and report the results in a future publication.

ACKNOWLEDGMENTS

The authors would like to thank Dr. F. G. J. Perey, Dr. R. E. Schenter, Dr. C. W. Lindenmeier, Dr. B. R. Leonard, Jr., Dr. R. L. Cassola, and Dr. G. I. Harris for many helpful discussions. The hospitality of Dr. Harris and the Aerospace Research Laboratories was greatly appreciated.

---

*Based on work performed under U. S. Atomic Energy Commission Contract No. AT(45-1)-1830.

†Present address: Aerospace Research Laboratories, Wright-Patterson Air Force Base, Ohio 45433.

‡Part of the research was performed at the U.S.A.F. Aerospace Research Laboratories while in the capacity of an Ohio State University Research Foundation Visiting Research Associate under Contract No. F33615-67-C-1758.

§Present address: Los Alamos Scientific Laboratory, Los Alamos, New Mexico 87544.

[1]D. G. Foster, Jr., and D. W. Glasgow, preceding paper [Phys. Rev. C 3, 576 (1971)].

[2]D. W. Glasgow and D. G. Foster, Jr., Phys. Rev. Letters 22, 139 (1969).

[3]D. W. Glasgow and D. G. Foster, Jr., Bull. Am. Phys. Soc. 14, 39 (1969).

[4]F. Perey and B. Buck, Nucl. Phys. 32, 353 (1962).

[5]H. Feshbach, Ann. Phys. (N.Y.) 5, 357 (1958); R. E. Schenter, Nucl. Phys. A94, 408 (1967).

[6]A. Bohr and B. R. Mottelson, in *Nuclear Structure* (W. A. Benjamin, Inc., New York, 1969), Vol. 1, p. 218.

[7]T. Tamura, Rev. Mod. Phys. 37, 679 (1965).

[8]J. T. Reynolds, C. J. Slavik, C. R. Lubitz, and N. C. Francis, Phys. Rev. 176, 1213 (1968).

[9]G. E. Brown, in *Proceedings of the International Congress on Nuclear Physics, Paris, 1964,* edited by P. Gugenberger (Centre National de la Recherche Scientifique, Paris, France, 1964), Vol. I, p. 129.

[10]B. Block and H. Feshbach, Ann. Phys. (N.Y.) 23, 47

(1963); A. K. Kerman, L. S. Rodberg, and J. E. Young, Phys. Rev. Letters 11, 422 (1963); R. H. Lemmer and C. M. Shakin, Ann. Phys. (N.Y.) 27, 13 (1964); A. Lande and B. Block, Phys. Rev. Letters 12, 334 (1964); H. Feshbach, Rev. Mod. Phys. 36, 1076 (1964); H. Feshbach, A. K. Kerman, and R. H. Lemmer, Ann. Phys. (N.Y.) 41, 230 (1967).

[11]T. Ericson, Ann. Phys. (N.Y.) 23, 390 (1963).

[12]I. R. Afnan, Phys. Rev. 163, 1016 (1967).

[13]J. Bar-Touv and A. Goswami, Phys. Letters 28B, 391 (1969).

[14]H. Feshbach, Ann. Phys. (N.Y.) 19, 287 (1962).

[15]J. D. McCullen, B. F. Bayman, and L. Zamick, Phys. Rev. 134, B515 (1964).

[16]L. S. Kisslinger and R. A. Sorenson, Rev. Mod. Phys. 35, 853 (1963).

[17]R. K. Sheline, T. Sikkeland, and R. N. Chanda, Phys. Rev. Letters 7, 446 (1961).

[18]E. Marshalek, L. W. Person, and R. K. Sheline, Rev. Mod. Phys. 35, 108 (1963).

[19]K. Kumar and M. Baranger, Phys. Rev. Letters 12, 73 (1964).

[20]F. Ackermann, E. W. Otten, G. ZuPutlitz, A. Schenck, and S. Ullrich, Phys. Letters 26B, 367 (1968).

[21]K. Kumar and M. Baranger, Nucl. Phys. A110, 529 (1968).

[22]M. Sakai, Nucl. Phys. A104, 301 (1967).

[23]H. Marshak, A. Langsford, C. Y. Wong, and T. Tamura, Phys. Rev. Letters 20, 554 (1968).

[24]D. M. Chase, L. Wilets, and A. R. Edmonds, Phys. Rev. 110, 1080 (1958).

[25]B. Buck and F. Perey, Phys. Rev. Letters 8, 444 (1962).

[26]B. Baldoni and A. M. Saruis, Nuovo Cimento 33, 1145 (1964).

[27]N. K. Glendenning, in *Nuclear Structure and Nuclear Reactions, Proceedings of the International School of Physics "Enrico Fermi," Course XL,* edited by M. Jean (Academic Press Inc., New York, 1969).